HPU2 Journal of Sciences:
Natural Sciences and Technology

Journal homepage: https://sj.hpu2.edu.vn

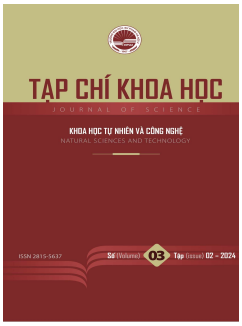

Article type: Research article

Structure, magnetic properties and magnetocaloric effect of $Fe_{81-x}Cr_{x+4}B_2Zr_{10}Nd_3$ rapidly quenched alloys

Hai-Yen Nguyen[a*], Huy-Ngoc Nguyen[a], Xuan-Hau Kieu[a], Thi-Thanh Pham[a], Viet-Anh Truong[a], Dinh-Thang Duong[b], Van-Duong Nguyen[b], Huy-Dan Nguyen[a]

[a]*Institute of Materials Science - VAST, Hanoi, Vietnam*
[b]*Hanoi Pedagogical University 2, Vinh Phuc, Vietnam*

Abstract

This paper presents, we present the structure, magnetic properties, and magnetocaloric effect of the $Fe_{81-x}Cr_{x+4}B_2Zr_{10}Nd_3$ (x = 0, 1, 2, and 3) alloy ribbons. The alloy ribbons were prepared by using the melt-spinning method. Structural analysis by X-ray diffraction shows that the obtained alloy ribbons are almost amorphous. Curie temperature of the alloy ribbons decreases from 310 to 275 K when x increases from 0 to 3. Under a magnetic field change of 12 kOe, the maximum magnetic entropy change ($|\Delta S_m|_{max}$) of the $Fe_{80}Cr_5B_2Zr_{10}Nd_3$ alloy ribbon is found to be 1.05 $J.kg^{-1}.K^{-1}$ at 302 K. In addition, the large refrigerant capacity (RC > 80 $J{\cdot}kg^{-1}$ with ΔH = 12 kOe) at room temperature is obtained in the alloy ribbon. Thus, the alloy ribbons can be considered a potential magnetic refrigerant in the room temperature range.

Keywords: Magnetocaloric effect, magnetic entropy change, refrigerant capacity, magnetic refrigerant, melt-spinning method

1. Introduction

Today, global warming and rising energy costs of energy require the development of new cooling technologies to replace conventional gas-compression/expansion refrigeration. In response to this demand, the magnetic refrigeration (MR) technology based on the magnetocaloric effect (MCE) of the material, which is characterized by an isothermal magnetic entropy change ($\Delta S_m(T)$), an adiabatic temperature change ($\Delta T_{ad}(T)$) and a refrigerant capacity (RC), is a good candidate. This technology has attracted more and more attention because the MR has greater cooling efficiency, lower energy consumption, and higher

* Corresponding author, E-mail: yennh@ims.vast.ac.vn

https://doi.org/10.56764/hpu2.jos.2024.3.2.10-17

Received date: 28-02-2024 ; Revised date: 03-4-2024 ; Accepted date: 10-4-2024

environmental safety than conventional gas refrigeration [1]–[2]. Therefore, magnetocaloric materials have been increasingly interested in research and development over the past few decades [1]–[10].

The magnetocaloric materials can be divided into two categories: the materials that undergo first-order magnetic phase transition (FOMPT) usually have a giant ΔS_m over a narrow temperature range [3]–[11]; the materials undergoing the second-order magnetic phase transition (SOMPT) show that the $\Delta S_m(T)$ peak expands around the phase transition temperature [10], [12–15]. The SOMPT material is considered more suitable for application in the MR because of its wide working temperature range (usually greater than 50 K) [12]–[14]. Among SOMPT materials, Fe-Zr-based amorphous alloys display almost all features of an ideal magnetic refrigerant in the room temperature region, such as large $\Delta S_m(T)$ peak over a wide temperature range, good mechanical properties, low price, adjustable magnetic transition Curie temperature (T_C). To improve the glass forming ability (GFA), MCE, and tune T_C and for these materials, other elements such as Co, B, Cr, Mn, and Nd have been incorporated [12]–[16]. For example, the T_C phase transition temperature of the alloy $(Fe_{0.95}M_{0.05})_{0.9}Zr_{0.1}$ was adjusted to the region room temperature by adding elements [1]. The saturation magnetization (M_s), the T_C, and the MCE of $Fe_{92-x}Zr_8B_x$ alloy ribbons were significantly improved by the addition of B [14]. The T_C of these alloy ribbons increased from 291 K (for $x = 3$) to 306 K (for $x = 5$) with increasing B-concentration. The maximum magnetic entropy change ($|\Delta S_m|_{max}$) of the $Fe_{87}Zr_8B_4$ alloy ribbon reaches 0.88 $J.kg^{-1}.K^{-1}$ at 291 K [14]. The replacement of a small amount of Co for Fe gives more increment in the T_C and the $|\Delta S_m|_{max}$ of the $Fe_{88-x}Zr_{11}B_1Co_x$ ($x = 1, 2$) amorphous alloys [16]. For an applied field of 15 kOe, the sample with x = 2 exhibits a large $|\Delta S_m|_{max}$ of 1.73 $J.kg^{-1}.K^{-1}$, and a high refrigerant capacity (RC) of 124 $J.kg^{-1}$ at 300 K [16]. In addition, The T_C of Fe-Zr-based amorphous alloys can be reduced to room temperature with the substitution of Cr for Fe [17], [18]. GFA of Fe-Zr-based alloys also considerably improves with the addition of Cr. With a magnetic field change of 15 kOe, the $Fe_{80}Cr_4B_{10}Zr_5Gd_1$ alloy with 4 at% Cr-concentration presented high RC (110 $J.kg^{-1}$) [17]. Thus, one can see that the influence of the additional elements on the T_C, GFA, and MCE of the Fe-Zr-based alloys is widely varied. Therefore, to improve their GFA, MCE and adjust the T_C of the alloy to room temperature region, we investigated the influence of Cr on structure, magnetic properties and MCE of $Fe_{81-x}Cr_{x+4}B_2Zr_{10}Nd_3$ ($x = 0$, 1, 2, and 3) alloy ribbons.

2. Experimental section

The bulk alloys with $Fe_{81-x}Cr_{x+4}B_2Zr_{10}Nd_3$ (x = 0, 1, 2, and 3) compositions were prepared from pure metals of Fe, Cr, Nd, B, and Zr (> 99%) by using an arc-melting method. To prevent oxidation, the alloy ingots were prepared in an arc furnace in Ar gas. Each sample was remelted and turned five times to ensure the homogeneity of the alloys. The alloy ingots were then fabricated on a single-wheel melt-spinning system in a purified Argon atmosphere. The obtained ribbons had thicknesses and widths of about 50 μm and 3 mm, respectively. The structure of the samples at room temperature was examined by using X-ray diffraction (XRD). The magnetization versus temperature and magnetic field were carried out on the ribbon samples using a vibrating sample magnetometer (VSM).

3. Results and discussion

Structure of $Fe_{81-x}Cr_{x+4}B_2Zr_{10}Nd_3$ ($x = 0$, 1, 2, and 3) alloy ribbons are analyzed by using XRD. From the XRD pattern (Figure 1), we observe only one diffraction peak around $2\theta \approx 43°$. By qualitative analysis of the crystal phase, we see that this diffraction peak is similar to the (110) lattice plane of the α-Fe phase. This can be a demonstration of the existence of a nanocrystalline phase whose structure is close to that of α-Fe is dispersed on the $Fe_{81-x}Cr_{x+4}B_2Zr_{10}Nd_3$ alloy ribbons. However, the intensity of

this peak is relatively weak and decreases when *x* increases. This means that the GFA of the alloy ribbons is significantly improved with the increase of the concentration of Cr. The alloy ribbons are almost amorphous. Similar results were observed in the other Fe-Zr-based alloys such as Fe-Ni-Zr [19], Fe-B-Zr [14], and Fe-Sn-Zr [20].

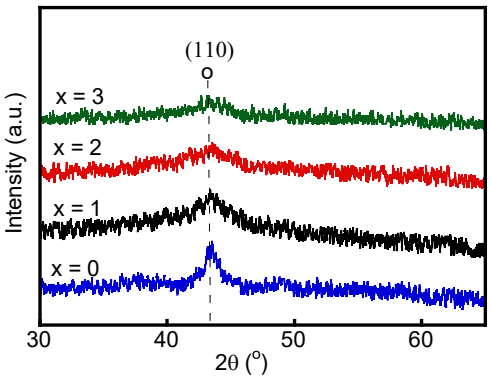

Figure 1. Room-temperature XRD pattern of Fe81-xCrx+4B2Zr10Nd3 (x = 0, 1, 2, and 3) alloy ribbons.

Figure 2. shows hysteresis loops measured at room temperature for $Fe_{81-x}Cr_{x+4}B_2Zr_{10}Nd_3$ (x = 0, 1, 2, and 3) alloy ribbons. One can see that all the alloy ribbons exhibited soft magnetic. This is good for magnetic refrigeration because the magnetic hysteresis loss should be very small or negligible. Besides, the maximum magnetization at the magnetic field of 12 kOe ($M_{12\ kOe}$) of the samples is reduced with increasing Cr concentration. The value $M_{12\ kOe}$ is 38.8, 35.1, 25.1, and 21.3 emu/g for x = 0, 1, 2, and 3, respectively.

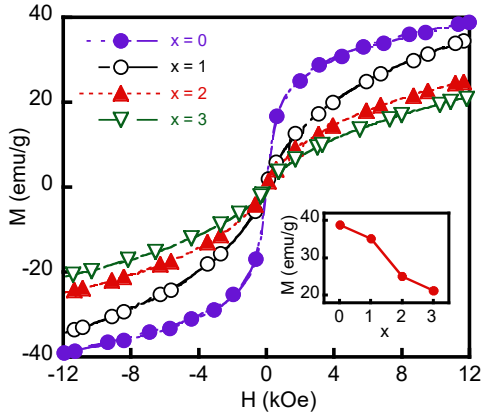

Figure 2. Hysteresis loops at room temperature of $Fe_{81-x}Cr_{x+4}B_2Zr_{10}Nd_3$ (x = 0, 1, 2, and 3) alloy ribbons.

The magnetic phase transition temperatures are an important factor for choosing the magnetocaloric material because the MCE of a material achieves its maximum value around these temperatures. Figure 3.a presents the reduced thermomagnetic curves $M(T)$ of $Fe_{81-x}Cr_{x+4}B_2Zr_{10}Nd_3$ (x = 0, 1, 2, and 3) alloy ribbons measured in an applied magnetic field of 100 Oe. The samples have a fairly sharp magnetic phase transition. This phase transition corresponds to the amorphous phase in the alloy ribbons. After the magnetic phase transition, except for sample x = 0, the magnetization of other samples decreased nearly to zero. This proves that the sample x = 0 is not monophasic. This is in agreement with the structural analysis above. On the other hand, we can see that as in the previous section, the concentration of Cr has a significant effect on the T_C of the alloy ribbons. The T_C of the samples is determined from

the minimum of the dM/dT versus T curves (Figure 3.b). The T_C of samples ranges from 275 to 310 K, depending on the concentration of Cr. This value decreases with increasing Cr concentration. According to previous studies [17], [18], it has been assumed that an antiferromagnetic coupling exists between Fe and Cr. This antiferromagnetic coupling causes to weaken the ferromagnetic coupling. Hence, the T_C of the alloy ribbons reduces with increasing the concentration of Cr (see the inset of Figure 3.b). The T_C value determined for samples x = 0, 1, 2, and 3 is 310, 302, 285, and 275 K, respectively. Thus, the T_C of the alloy ribbons has been gradually adjusted to room temperature when the concentration of Cr increases.

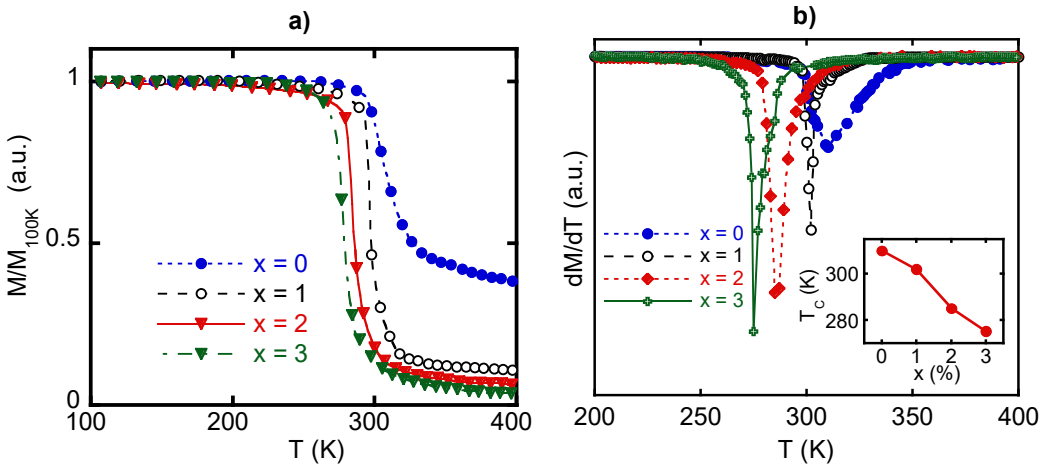

Figure 3. Temperature dependences of **a**) magnetization M and **b**) dM/dT of $Fe_{81-x}Cr_{x+4}B_2Zr_{10}Nd_3$ (x = 0, 1, 2, and 3) alloy ribbons in the applied magnetic field of 100 Oe. The inset shows the Curie temperature T_C versus Cr of these samples.

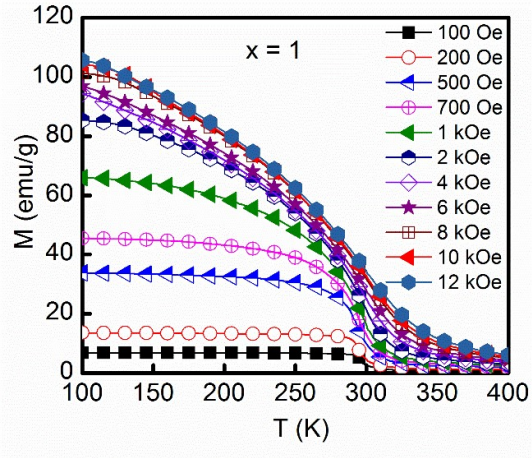

Figure 4. Thermomagnetization curves in various magnetic fields of $Fe_{80}Cr_5B_2Zr_{10}Nd_3$ alloy ribbon.

According to the results of the above analyses, the sample with x = 1 is quite monophasic and has a phase transition temperature at room temperature. Therefore, we have selected this sample to investigate the MCE of the alloy. The MCE of the alloy ribbons is evaluated using their magnetic entropy change, ΔS_m. Figure 4. presents the thermomagnetization curves of $Fe_{80}Cr_5B_2Zr_{10}Nd_3$ ribbon at different magnetic fields in the range of 100 Oe to 12 kOe. We can observe that the magnetization of the alloy ribbons

increases with increasing the magnetic field. All the thermomagnetization curves have an almost unchanged T_C phase transition temperature of around 300 K.

To better understand the nature of the magnetic phase transition and the magnetic order in the alloy ribbons, the Arrott plots (M^2-H/M) were constructed from $M(H, T)$ data (Figure 5.a). According to Banerjee's criteria [1]–[2], the sign of the slope of the M^2-H/M curves (Figure 5.b) tells us the nature of the phase transition. The negative slope corresponds to the first-order magnetic phase transition (FOMPT), and the positive slope corresponds to the second-order magnetic phase transition (SOMPT). From Figure 5.b, we see that all the M^2-H/M curves of these samples have positive slopes. This proves that the magnetic phase transition occurring on the sample belongs to the SOMPT.

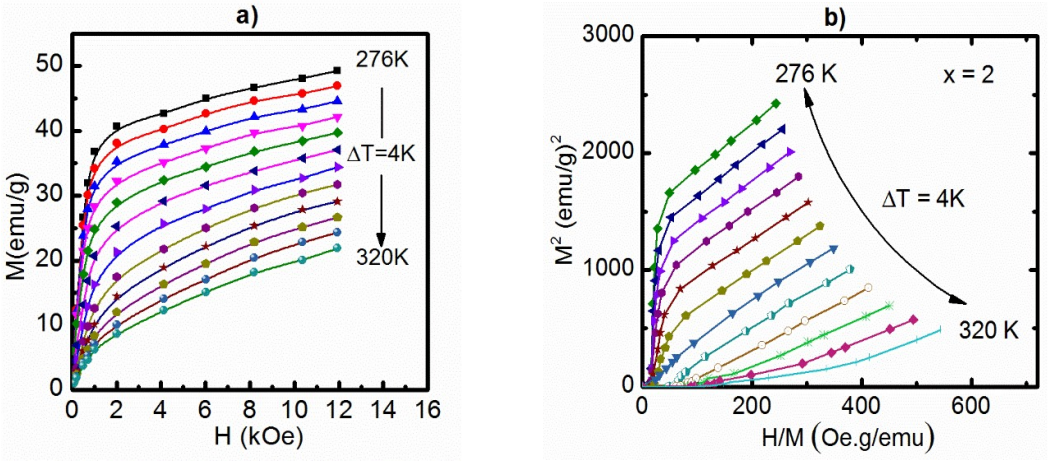

Figure 5. Magnetization vs. the magnetic field **(a)** and the M^2-H/M plots **(b)** at various temperatures ranging from 276 K to 320 K with temperature step (ΔT) of 4 K of the representative $Fe_{80}Cr_5B_2Zr_{10}Nd_3$ alloy ribbon.

The ΔS_m values of the $Fe_{80}Cr_5B_2Zr_{10}Nd_3$ alloy ribbon are indirectly calculated from the $M(H, T)$ data (Figure 5.a) using the following Maxwell equation [1] –[2]:

$$\Delta S_m = \int_0^H \left(\frac{\partial M}{\partial T}\right)_H dH \quad (1)$$

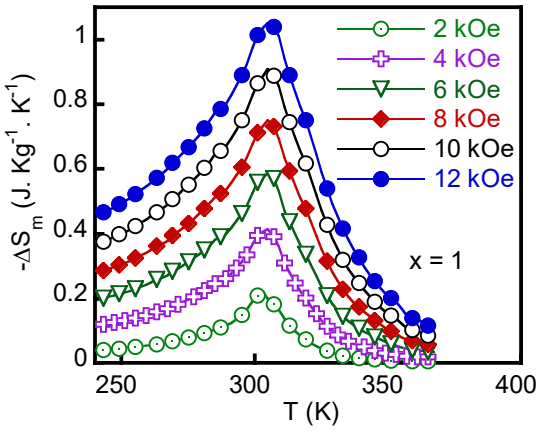

Figure 6. The $-\Delta S_m(T)$ plots in various magnetic field changes of $Fe_{80}Cr_5B_2Zr_{10}Nd_3$ alloy ribbon.

Figure 6. shows the -$\Delta S_m(T)$ curves in various magnetic field changes (ΔH) up to 12 kOe (ΔH = 2, 4, 6, 10 and 12 kOe) of the $Fe_{80}Cr_5B_2Zr_{10}Nd_3$ alloy ribbon. The results show that the sample has negative ΔS_m, and reached high values around the magnetic phase transition temperature. Besides, the $|\Delta S_m|_{max}$ value of the sample increases with increasing of ΔH. With the highest magnetic field change from 0 to 12 kOe (ΔH = 12 kOe), the $|\Delta S_m|_{max}$ value of the sample is 1.05 $J.kg^{-1}.K^{-1}$ at 302 K (Figure 7.). This value is equivalent or higher than that of other Fe-Zr-based alloys such as $Fe_{76}Cr_8B_{10}Zr_5Gd_1$ ($|\Delta S_m|_{max}$ = 0.66 $J.kg^{-1}.K^{-1}$ with ΔH = 15 kOe) [17], $Fe_{88}Zr_8B_4$ ($|\Delta S_m|_{max}$ = 0.87 $J.kg^{-1}.K^{-1}$ with ΔH = 10 kOe) [21], $Fe_{90}Zr_9Cu_1$ ($|\Delta S_m|_{max}$ = 0.75 $J.kg^{-1}.K^{-1}$ with ΔH = 10 kOe) [22], and $Fe_{89}Zr_8B_3$ ($|\Delta S_m|_{max}$ = 0.79 $J.kg^{-1}.K^{-1}$ with ΔH = 10 kOe) [14].

In addition, to evaluate the applicability of magnetocaloric materials, it is often referred to as the refrigerant capacity (RC). The RC is determined by the following formula:

$$RC = |\Delta S_m|_{max} \times \delta T_{FWHM} \quad (2)$$

where, δTFWHM is the full width at half maximum of the -ΔSm(T) curves, which is referred to as the working temperature range of a magnetic refrigerant. With ΔH = 12 kOe (the magnetic field changes from 0 to 12 kOe), the δTFWHM value of the sample is 87 K.

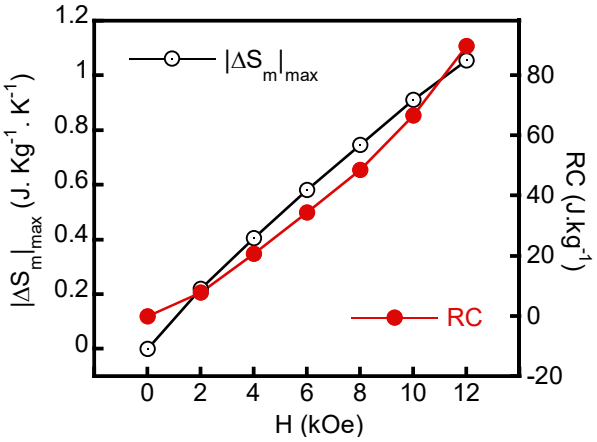

Figure 7. Field dependence of $|\Delta S_m|_{max}$ **(a)** and RC **(b)** of the $Fe_{80}Cr_5B_2Zr_{10}Nd_3$ alloy ribbon.

The field dependence of RC of the alloy ribbons in various magnetic field changes of 0 - 12 kOe is presented in Figure 7. The result shows that the RC of the sample was quite high. With ΔH = 12 kOe, the largest RC value of the $Fe_{80}Cr_5B_2Zr_{10}Nd_3$ alloy ribbon is 91 $J.kg^{-1}$. These values are comparable to other amorphous alloys such as $Fe_{84-x}Cr_xB_{10}Zr_5Gd_1$ [17], $Fe_{88-x}Zr_8B_4Mn_x$, $Fe_{88-x}Zr_8B_4Er_x$ [23], and greater than the value of some other crystalline amorphous and nano-crystalline alloys such as $Fe_{83-x}Co_xZr_6B_{10}Cu_1$, $Fe_{91-x}Mo_8Cu_1B_x$, $Fe_{60-x}Mn_xCo_{18}Nb_6B_{16}$ [24], $Fe_{86}Sn_4Zr_{10}$ [20].

4. Conclusions

Thus, Cr has a considerable influence on the structure, magnetic properties, and magnetocaloric effect of the $Fe_{81-x}Cr_{x+4}B_2Zr_{10}Nd_3$ (x = 0, 1, 2, and 3) alloy ribbons. The increase of the Cr concentration improved the GFA of the alloy ribbons. The T_C of the alloy ribbons is shifted to room temperature with the appropriate Cr concentration. The magnetic phase transition occurring in the $Fe_{80}Cr_5B_2Zr_{10}Nd_3$ alloy ribbon belongs to the second-order magnetic phase transition. The obtained values of $|\Delta S_m|_{max}$ and RC

are quite large (1.05 $J.kg^{-1}.K^{-1}$ and 91 $J.kg^{-1}$ with ΔH = 12 kOe) at room temperature. This shows that the applicability of the alloy ribbons in magnetic refrigerant technology is very high.

Acknowledgments

This work was supported by Institute of Materials Science, Vietnam Academy of Science and Technology under grant number CSCL04.01/24-25. Hai-Yen Nguyen was funded by the Postdoctoral Scholarship Programme of Vingroup Innovation Foundation (VINIF), code VINIF.2023.STS.67. A part of the work was done in the Key Laboratory for Electronic Materials and Devices, Institute of Materials Science, VAST, Viet Nam.

References

[1] V. Franco, J. S. Blázquez, J. J. Ipus, J. Y. Law, L. M. Moreno-Ramírez, and A. Conde, "Magnetocaloric effect: From materials research to refrigeration devices," *Prog. Mater. Sci.,* vol. 93, pp. 112–232, Apr. 2018, doi: 10.1016/j.pmatsci.2017.10.005.

[2] A. M. Tishin, Y. I. Spichkin, V. I. Zverev, and P. W. Egolf, "A review and new perspectives for the magnetocaloric effect: New materials and local heating and cooling inside the human body," *Int. J. Refrig.,* vol. 68, pp. 177–186, Aug. 2016, doi: 10.1016/j.ijrefrig.2016.04.020.

[3] N. Tiwari, V. Pal, S. Das, and M. Paliwal, "Proposed compositions in a Ni-Mn-Ga system for magnetocaloric applications," *J. Electron. Mater.,* vol. 53, no. 4, pp. 1773–1795, Jan. 2024, doi: 10.1007/s11664-023-10882-0.

[4] Yu. S. Koshkid'ko *et al.*, "Magnetocaloric effect and magnetic phase diagram of Ni-Mn-Ga Heusler alloy in steady and pulsed magnetic fields," *J. Alloys Compd.,* vol. 904, p. 164051, May 2022, doi: 10.1016/j.jallcom.2022.164051.

[5] P. Lázpita, A. Pérez-Checa, J. M. Barandiarán, A. Ammerlaan, U. Zeitler, and V. Chernenko, "Suppression of martensitic transformation in Ni-Mn-In metamagnetic shape memory alloy under very strong magnetic field," *J. Alloys Compd.,* vol. 874, p. 159814, Sep. 2021, doi: 10.1016/j.jallcom.2021.159814.

[6] T. Bachagha, R. Chakaravarthy, W. Ren, J. Saurina, and J.-J. Suñol, "Structural, magnetocaloric, and magnetic properties in Heusler $Ni_{50}Mn_{35}In_{10}X_5$ (X = Ga, Fe and Al) alloys," *Metals,* vol. 13, no. 12, p. 1913, Nov. 2023, doi: 10.3390/met13121913.

[7] Y. Zhang, J. Ouyang, X. Wang, Y. Tian, and Z. Ren, "Magneto-structural transformations and magnetocaloric effect in the Heusler type $Ni_{48}Cu_2Mn_{36}Sn_{14-x}Ti_x$ melt-spun ribbons," *Mater. Chem. Phys.,* vol. 290, p. 126527, Oct. 2022, doi: 10.1016/j.matchemphys.2022.126527.

[8] F. Wang *et al.*, "Effect of sintering temperature on the magnetocaloric effect of Ni-Mn-In/Tb-Dy-Fe composites," *J. Supercond. Nov. Magn.,* vol. 37, no. 3, pp. 557–563, Jan. 2024, doi: 10.1007/s10948-024-06695-9.

[9] J. Sharma, A. A. Coelho, K. G. Suresh, and A. Alam, "Martensitic and room-temperature magnetocaloric properties of Mn-rich Mn-Ni-Sn Heusler alloys: Experiment and theory," *Phy. Rev. B,* vol. 109, no. 6, p. 064418, Feb. 2024, doi: 10.1103/PhysRevB.109.064418.

[10] D. D. Kuznetsov *et al.,* "Magnetocaloric effect, structure, spinodal decomposition and phase transformations Heusler alloy Ni-Mn-In," *Nanomaterials,* vol. 13, no. 8, p. 1385, Apr. 2023, doi: 10.3390/nano13081385.

[11] F. Zhang *et al.*, "The second-order magnetic phase transition and magnetocaloric effect in all-d-metal NiCoMnTi-based Heusler alloys," *J. Alloys Compd.,* vol. 906, p. 164337, Jun. 2022, doi: 10.1016/j.jallcom.2022.164337.

[12] A. L. Li, Q. Wang, B. Z. Tang, P. Yu, D. Ding, and L. Xia, "Magnetocaloric effect of the $Fe_{87}M_8B_5$ (M = Zr, Ce) amorphous alloys," *Mater. Sci. Eng. B,* vol. 286, p. 116033, Dec. 2022, doi: 10.1016/j.mseb.2022.116033.

[13] Q. Wang, D. Ding, B. Z. Tang, P. Yu, K. C. Chan, and L. Xia, "Excellent magnetocaloric performance of a $Fe_{88}Zr_4Pr_4B_4$ amorphous alloy and its amorphous hybrids," *Intermetallics,* vol. 161, p. 107982, Oct. 2023. doi: 10.1016/j.intermet.2023.107982.

[14] X. Wang, Q. Wang, B. Z. Tang, D. Ding, L. Cui, and L. Xia, "Magnetic and magneto-caloric properties of the amorphous $Fe_{92-x}Zr_8B_x$ ribbons," *Materials (Basel).,* vol. 13, no. 23, p. 5334, Nov. 2020, doi: 10.3390/ma13235334.

[15] B. Biswas, D. Biswas, M. Debnath, E. Bose, and S. Pal, "Giant magnetocaloric effect and second order phase

transition in $PrMnO_3$," *J. Magn. Magn. Mater.,* vol. 588, p. 171445, Dec. 2023, doi: 10.1016/j.jmmm.2023.171445.

[16] X. Li, Y. Pan, and T. Lu, "Magnetocaloric effect in Fe-based amorphous alloys and their composites with low boron content," *J. Non-Cryst. Solids,* vol. 487, pp. 7–11, May 2018, doi: 10.1016/j.jnoncrysol.2018.02.022.

[17] D. Guo, K. C. Chan, and L. Xia, "Influence of minor addition of Cr on the magnetocaloric effect in Fe-based metallic ribbons," *Mater. Trans.,* vol. 57, no. 1, pp. 9–14, Jan. 2016, doi: 10.2320/matertrans.M2015146.

[18] Y. K. Fang *et al.*, "Magnetocaloric effect in Fe-Zr-B-M (M = Mn, Cr, and Co) amorphous systems," *J. Appl. Phys.,* vol. 105, no. 7, p. 093910, Feb. 2009, doi: 10.1063/1.3054369.

[19] T. D. Thanh *et al.*, "Critical behavior of the ferromagnetic-paramagnetic phase transition in $Fe_{90-x}Ni_xZr_{10}$ alloy ribbons," *J. Appl. Phys.,* vol. 115, no. 2, p. 023903, Jan. 2014, doi: 10.1063/1.4861400.

[20] T. L. Phan *et al.*, "Magnetic properties and magnetocaloric effect in $Fe_{90-x}Sn_xZr_{10}$ alloy ribbons," *J. Korean Phys. Soc.,* vol. 66, no. 8, pp. 1247–1252, Apr. 2015, doi: 10.3938/jkps.66.1247.

[21] L. Chen, J. Zhang, L. Wen, P. Yu, and L. Xia, "Outstanding magnetocaloric effect of $Fe_{88-x}Zr_8B_4Sm_x$ (x=0, 1, 2, 3) amorphous alloys," *Sci. China Phys. Mech. Astron.,* vol. 61, no. 5, p. 056121, Nov. 2018, doi: 10.1007/s11433-017-9152-7.

[22] W. Yang *et al.*, "Low-temperature magnetic properties and magnetocaloric effect of Fe–Zr–Cu amorphous alloys," *J. Low Temp. Phys.,* vol. 200, no. 1, pp. 51–61, May 2020, doi: 10.1007/s10909-020-02452-z.

[23] D. Q. Guo, Y. D. Yuan, and K. C. Chan, "The effect of different minor additions on the magneto-caloric effect of FeZrB metallic ribbons near room temperature," *J. Magn. Magn. Mater.,* vol. 446, pp. 12–17, Jan. 2018, doi: 10.1016/j.jmmm.2017.09.009.

[24] V. Franco, J. S. Blázquez, M. Millán, J. M. Borrego, C. F. Conde, and A. Conde, "The magnetocaloric effect in soft magnetic amorphous alloys," *J. Appl. Phys.,* vol. 101, no. 9, p.09c503, Mar. 2007, doi: 10.1063/1.2709409.